On the localization of artificial submarine groundwater discharge sites using a low-cost multi-sensor-platform

Christoph Tholen
Department of
Engineering Sciences
Jade University
of Applied Sciences
Wilhelmshaven, Germany
christoph.tholen@jade-hs.de

Robin Rofallski
Institute for Applied
Photogrammetry and
Geoinformatics
Jade University
of Applied Sciences
Oldenburg, Germany
robin.rofallski@jade-hs.de

Lars Nolle
Department of
Engineering Sciences
Jade University
of Applied Sciences
Wilhelmshaven, Germany
lars.nolle@jade-hs.de

Tarek A. El-Mihoub
Department of
Engineering Sciences
Jade University
of Applied Sciences
Wilhelmshaven, Germany
tarek.el-mihoub@jade-hs.de

Iain Parnum
Centre for Marine Science
and Technology
Curtin University
Perth, Australia
i.parnum@curtin.edu.au

Oliver Zielinski
ICBM, Center for Marine
Sensors, Wilhelmhaven,
University of Oldenburg
and
DFKI RG Marine
Perception, Oldenburg,
Germany
oliver.zielinski@uol.de

***Abstract*— In this paper, a low-cost, multi-sensor platform designed to investigate the spatial distribution of water quality properties is presented. The platform is based on an off-the-shelf underwater vehicle and various environmental sensors. Its intended application is the detection and mapping of submarine groundwater discharge (SGD), but it could be used for other related applications. In this study, an artificial submarine groundwater discharge (ASGD) was used to test the platform. Before the ASGD was installed, the study area was thoroughly surveyed using the platform developed to establish a baseline. After installation of the ASGD, the area was again thoroughly surveyed with the platform. The spatial and temporal variation in the data collected was used to evaluate the platform and sensors performances, and the usefulness of the different environmental parameters in mapping SGD. Although the experiments performed showed an influence of the ASGD on the measurements, this influence was smaller than expected. Different possible causes for this are discussed.**

Keywords*— *Multi-sensor-platform, Low-cost vehicle, Submarine groundwater discharge, environmental sensing

I. INTRODUCTION

The long-term goal of this research is to develop a flexible, autonomous low-cost platform for subsea exploration. The platform consists of an autonomous underwater vehicle (AUV) and an automated surface vehicle (ASV) [1]. Such platform could potentially be used for locating underwater objects, pollutants or natural phenomena, like dumped waste, lost harmful cargo or submarine groundwater discharges (SGD) [2].

In order to fulfill such tasks the spatiotemporal distribution of different substances concentrations needs to be determined on intermediate spatial scales (about several hundreds of square meters). ROVs and AUVs are well suited for these kinds of missions [3].

SGDs consist of a flow of fresh groundwater and, in some cases, the recirculation of seawater from the sea floor to the coastal ocean [2]. The fresh water and the sea water discharges commingle in the mixing zone (Fig. 1) [4]. The chemical composition of the inflow and physical parameters, e.g. temperature or electric conductivity, differ from the properties of coastal water [5, 6]. Due to these deviations, gradients in the different parameters occur in the surrounding of an SGD. This gradient information can be used by a search strategy in order to guide an autonomous underwater vehicle (AUV) towards the SGD [7]. In order to adapt such a search strategy to a real-world problem, ground truth data is required. Since locations of real SGDs are not easily accessible and the inflow varies over time [6], it is inappropriate to use real SGD data to test such search strategies. Hence, an artificial SGD (ASGD) was used in this study to evaluate the developed sensor tube and to observe ground truth data for the subsequent training of different search algorithms.

Parameters that have been used to locate and examine SGDs include salinity [6], radon [8], temperature [6] and the concentration of fluorescent dissolved organic matter (FDOM) [9], which is a surrogate for Colored Dissolved Organic Matter (CDOM). Some of these parameters have been used to determine the inflow rate or the composition of the inflow.

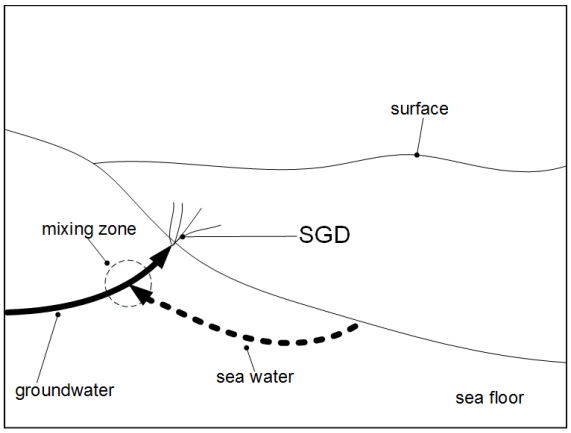

Fig. 1. Submarine Groundwater Discharge of Fresh- and Recirculating-Water, modified after [4].

However, if a small AUV is used as a platform, some of the aforementioned parameters cannot be used because the currently available sensors are too heavy or the response time of the sensors is too long [8]. Other parameters, like nutrient concentrations, require laboratory analysis. Furthermore, the risk of loss is imminent with AUVs. Therefore, there is a risk that sensors could be lost or damaged, which makes the utilization of low-cost sensors more appealing.

II. Low-Cost-Multi-sensor-Plattform

The multi-sensor-platform used in this research is based on an off-the-shelf BlueROV 2 system equipped with a Short Baseline positioning-system (SBL) [9]. Furthermore, the platform carries seven different low-cost sensors in order to measure environmental parameters, which include temperature (T), pressure (P), electric conductivity (EC), dissolved oxygen (DO), oxidation-reduction-potential (ORP), pH, and FDOM concentration. The specifications of the used sensors are summarized in TABLE I. These sensors were placed into a sensor tube, developed during this research. The sensor tube stores the data, measured by the seven sensors combined with a timestamp for post processing. In addition, the sensor tube was connected to the vehicle via serial connection. This allows online use of the sensor readings by the implemented search algorithms during the mission [1]. Fig. 2 shows the sensor-system mounted on the payload-kit of the BlueROV 2.

The sensors were connected to a microcontroller. This microcontroller collects the readings from the different sensors and manages the communication requests from the ROV. Each sensor has its own controller unit, handling the respective sensor reading and the parameter value calculation. The sensor controllers, except the FDOM sensor controller, are connected to the microcontroller using the I²C-bus [10]. The digital transmission of the sensor values prevents the introduction of measurement noise during the transmission between the sensor controller and the central microcontroller. Due to the analog transmission of the measurement value of the FDOM sensor, the signal of this sensor needs to be filtered during the post processing, in order to minimize the effect of the measurement noise.

TABLE I. Summarized Sensor specifications.

Parameter	Specifications		
	Range	*Accuracy*	*Distributor*
Temperature	-5 – 50 °C	0.1 °C	BlueRobotics
Pressure	0 – 30 bar	0.2 bar	BlueRobotics
Dissolved Oxygen	0.01 – 100 mg/L	0.05 mg/L	Atlas Scientific
pH	0.001 – 14.000	0.002	Atlas Scientific
Oxidation-Reduction-Potential	-1019.9 – 1019.9 mV	1 mV	Atlas Scientific
Electric Conductivity	5 – 200,000 µS/m	2 %	Atlas Scientific
FDOM	0 – 200 µg/L QSE[a]	n.n.	Trios

[a.] QSE: quinine sulphate equivalent units [11]

The sampling frequency of the sensors was set to 0.5 Hz. The total cost of the sensor tube developed, excluding the costs of the FDOM sensor, is approximately €1,600.

Fig. 2. Sensor-system with the optical FDOM sensor (right) and the sensor tube containing the other sensors (left).

III. Experiments

The sensor system described above was used to determine the spatiotemporal distribution of discharged freshwater in the water column using an artificial submarine spring. The experiments were conducted at Fremantle Sailing Club in Western Australia (Fig. 3). The dimension of the investigated area was approximately 75 m x 65 m while the maximum water depth was about 2.5 m. The area is connected to the Indian Ocean and therefore the consistence of the water is similar to the open sea. However, since the investigated area is located in a harbor, the conditions are favorable, e.g. sheltered and shallow water, low currents and easily accessible.

Before the ASGD was deployed, a survey had been conducted providing a baseline for comparison. Fig. 4 depicts the track of the ROV during the survey of the baseline. The blue box indicates the jetty (Fig. 3, left), while the red dot indicates the starting point of the track. It can be observed from the track,

that the whole area under investigation was covered by the sensor system. Due to a pillar at the end of the jetty, multipath effects occur on the SBL data, thus distorting the estimated positions in a funnel-shaped manner, north of the pillar.

Subsequently, a water hose was placed on a fixed point in the survey area and fresh water was supplied for 145 minutes. The inflow rate of the ASGD was 14.6 l/min.

Fig. 3. Left: Area under investigation (Fremantle Sailing Club, Perth Australia); Right: Sensor platform during operation at the ASGD (orange buoy, image centre).

The composition of the inflow was determined by the sensor system before and after the survey. The mean values and the standard deviations of the different parameters are summarized in TABLE II. It can be observed from TABLE II, that the mean values of the parameters before and after the experiments have the same order of magnitude. The measurements indicate that, the parameter values of the inflow did not vary significantly during the experiment.

The ASGD was located at position x =13.3 m; y = 0.5 m (Fig. 3, right). The origin of the coordinate system is at the origin of the Waterlinked SBL system. The position of the ASGD was determined using a Leica TS 15 total station.

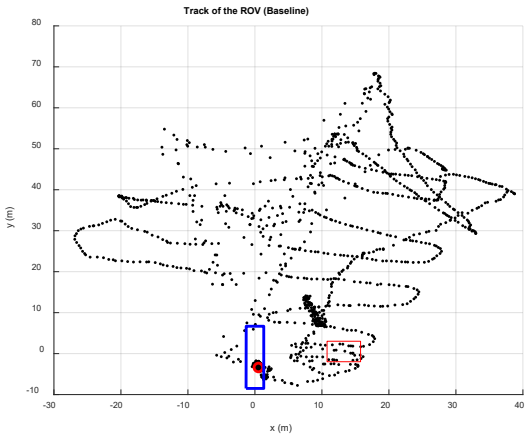

Fig. 4. Track of the ROV while surveying the baseline. Red rectangle marks the ASGD area; blue rectangle marks the jetty; red circle marks the starting point of the track.

TABLE II. MEAN VALUES AND STANDARD DEVIATIONS OF THE ARTIFICIAL FRESHWATER SPRING

Parameter	Before the Experiments		After the Experiments	
	Mean	*Standard-Deviation*	*Mean*	*Standard Deviation*
Temperature	23.7 °C	0.13 °C	24.6 °C	0.12 °C
Dissolved Oxygen	6.99 mg/L	0.36 mg/L	6.97 mg/L	0.42 mg/L
pH	8.15	0.14	8.61	0.06
Oxidation-Reduction-Potential	504.01 mV	22.92 mV	530.22 mV	50.02 mV
Electric Conductivity	0.445 mS/cm	0.014 mS/cm	0.599 mS/cm	0.018 mS/cm
FDOM	0.397 µg/L	0.091 µg/L	0.423 µg/L	0.102 µg/L

While the ASGD was in operation, the sensor platform was used to observe the changes in the environmental parameters within the investigated area. The entire area was covered thoroughly by several transects over a period of approx. 135 minutes. The track of the ROV is shown in Fig. 5. The position of the ASGD is marked by the red triangle. It can be observed from Fig. 5, that the whole area was covered by the ROV. However, the investigation was focused on the area of the ASGD.

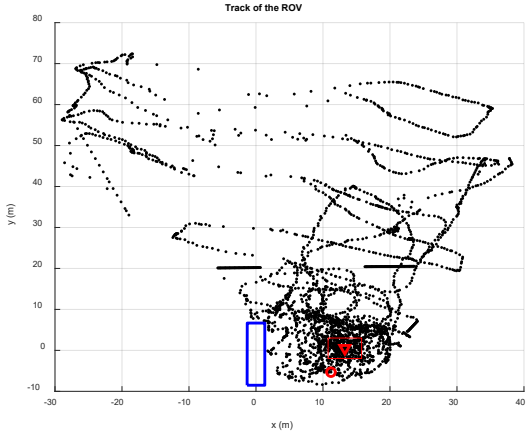

Fig. 5. Track of the ROV during the ASGD experiment. Red rectangle marks the ASGD area; blue rectangle marks the jetty; red circle marks the starting point of the track; red triangle marks the position of the ASGD.

The DO, pH, ORP, EC and FDOM mean values of the inflow (TABLE II) differ from the corresponding values of the water of the harbor. Hence, according to [6], it was assumed that the constant inflow of fresh water would reduce the electric conductivity in the immediate neighborhood of the source. Due to the decrease in the electric conductivity, also a decreasing salinity value is expected. Furthermore, the inflow should have an influence on the DO, pH, ORP, EC and FDOM values.

IV. RESULTS

Fig. 6 to Fig. 11 show the temporal changes of the environmental parameters (T, pH, ORP, EC, DO and FDOM) measured during the experiment. The data is divided into the baseline and the experiment, i.e. the time while the ASGD was

turned on. In addition, the data of the experiment is grouped into the points inside the area of the ASGD, i.e. data captured within the marked red box (Fig. 4 and Fig. 5), and the data outside this area. The blue dotted line at timestamp 6,000 seconds indicates high tide. Between timestamps 3,598 sec and 3,864 sec., no data was recorded due to a battery change for the ROV.

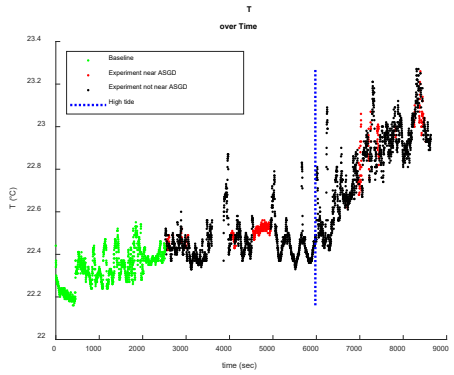

Fig. 6. Temperature over time separated into the data of the baseline (green) and data of the experiment inside the ASGD area (red) and outside (black).

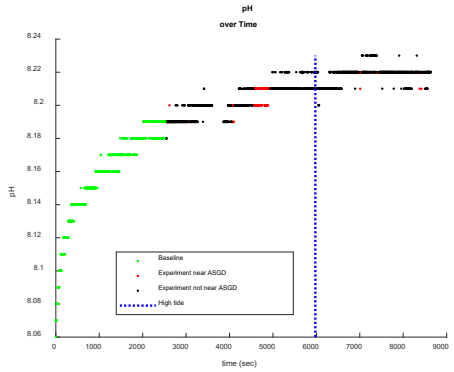

Fig. 7. pH over time separated into the data of the baseline (green) and data of the experiment inside the ASGD area (red) and outside (black).

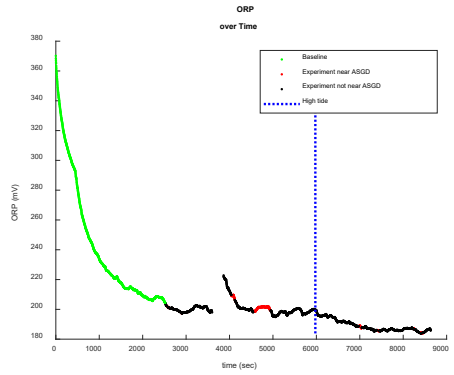

Fig. 8. ORP over time separated into the data of the baseline (green) and data of the experiment inside the ASGD area (red) and outside (black).

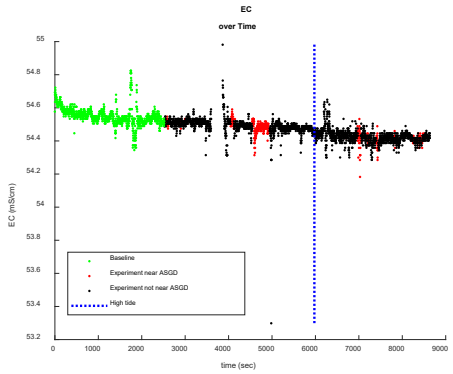

Fig. 9. EC over time separated into the data of the (green) and data of the experiment inside the ASGD area (red) and outside (black).

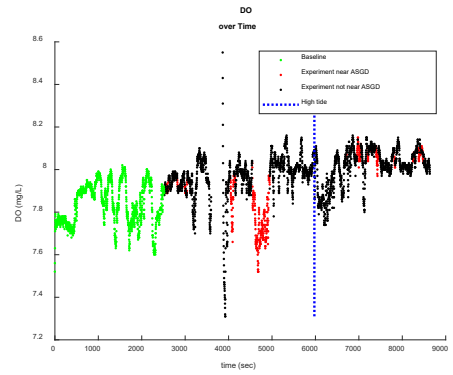

Fig. 10. DO over time separated into the data of the baseline (green) and data of the experiment inside the ASGD area (red) and outside (black).

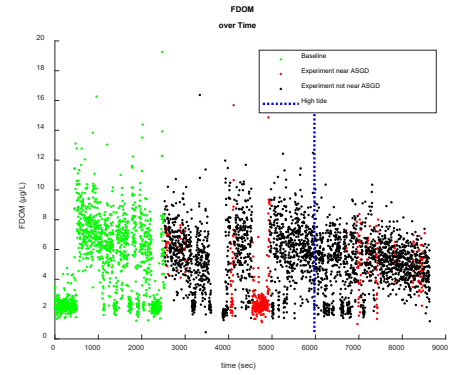

Fig. 11. FDOM over time separated into the data of the baseline (green) and data of the experiment inside the ASGD area (red) and outside (black).

During the post processing of the data, it was found that the EC-values are affected by a systematical measurement error, i.e. all values measured are lower than expected. Therefore, the EC data was corrected using a third-order polynomial correction function based on ten calibration solutions. The EC-values of these solutions were measured using the sensor tube and a calibrated lab device with an accuracy of 0.5 % [12]. The measured EC-values and the best-fit curve are shown in Fig. 12. The RMS error of the fit is 0.126 mS/cm.

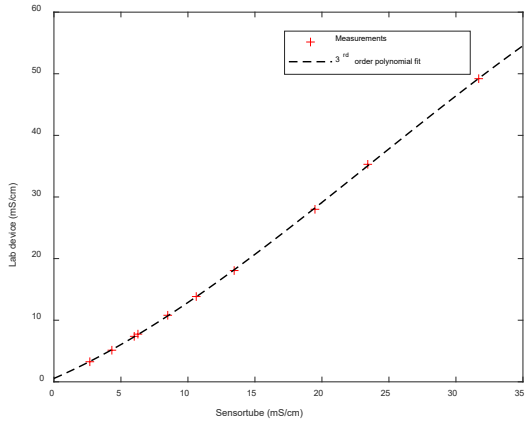

Fig. 12. EC post calibration thrid order polynomial fit

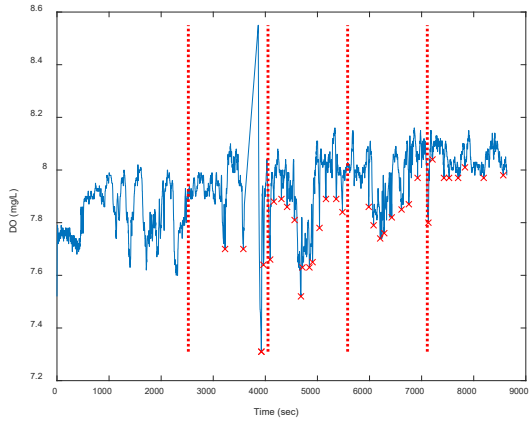

Fig. 13. DO over time, experiment data seperated in four time equal quarters, drops are marked with red crosses.

It can be observed from Fig. 6 that the temperature was increasing over time. It is likely that this increase was mainly caused by solar radiation. Another possible explanation could be the tide bringing warmer water into the harbor.

The pH values increased constantly over time (Fig. 7). The changes in the values are of the same order of magnitude as the sensor resolution, i.e. the value jumps from one bit to another. From the datasheet of the sensor, the resolution is expected one order of magnitude higher. Unfortunately, the used sensor tube does not support higher resolutions.

The ORP values decreased constantly from above 500 mV and stabilize after approximately 2,000 seconds at a value of around 200 mV (Fig. 8). A problem with the sensor can cause this behavior. Therefore, the ORP sensor seems unsuitable for this work. The EC decreased slowly during the experiments (Fig. 9).

Fig. 10 shows that the DO value increases slowly over time. However, between timestamps 4,500 and 5,000 sec., a significant drop in the DO value can be observed. During this time the ROV was hovering close to the ASGD. In addition, there are a couple of similar drops in the measured data. Fig. 13 shows the DO value over time. The total time of the experiment (except the baseline) was split into four equidistant time segments (red dashed lines). The dropping DO values are marked by the red crosses. The positions of the ROV at the time of these identified drops are shown in Fig. 14. It can be seen from Fig. 14 that a couple of the markers are in or close to the area of the ASGD. However, some of the positions are located far away from the ASGD.

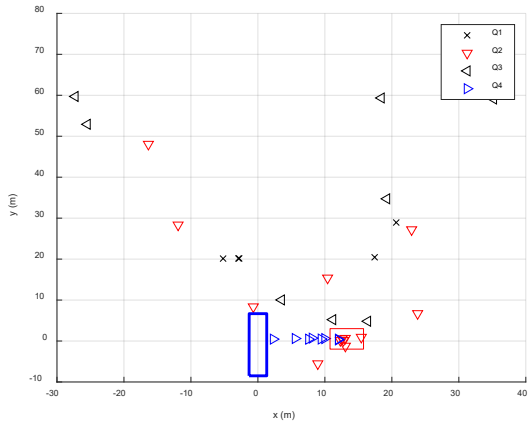

Fig. 14. Position of the ROV, during the drops of the DO value, clustered into the four time equal quarters.

Fig. 11 shows the readings of the FDOM sensor. It can be observed from Fig. 11 that the FDOM sensor readings are much more affected by measurement noise compared to the reading from the other sensors. In order to smooth the FDOM values, a median-filter with a window size of five was applied to the recorded FDOM data (Fig. 15 and Fig. 16). Fig. 16 shows the smoothed FDOM values together with the identified positions of the drops in the recorded DO data. The smoothed FDOM data shown (Fig. 15 and Fig. 16) had significant drops, similar to those seen in DO (Fig. 13). .

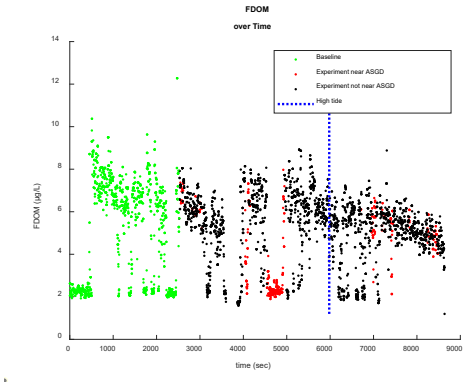

Fig. 15. Filtered FDOM over time separated into the data of the baseline (green) and data of the experiment inside the ASGD area (red) and outside (black)

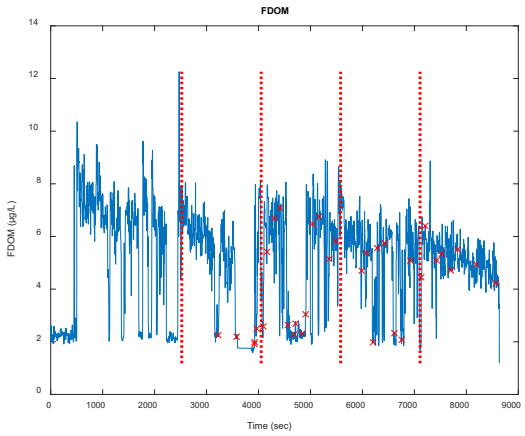

Fig. 16. Filtered FDOM over time (blue line) seperated in four time equal quarters together with the identified drops of the DO (red crosses)

The recorded T, EC, and P values were used to calculate the salinity [13]. Fig. 17 shows the calculated salinity over time. The data was divided using the same categories as described above. It can be observed from Fig. 17, that the salinity value decreased slowly over the first 6,000 seconds of the data recorded. Afterwards, the decreasing rate was higher. The change in the decreasing rate might have been affected by the tides.

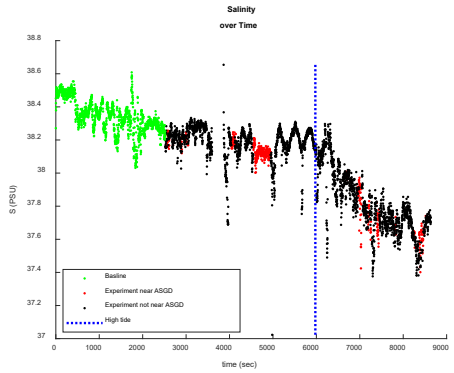

Fig. 17. Salinity over time separated into the data of the baseline (green) and data of the experiment inside the ASGD area (red) and outside (black).

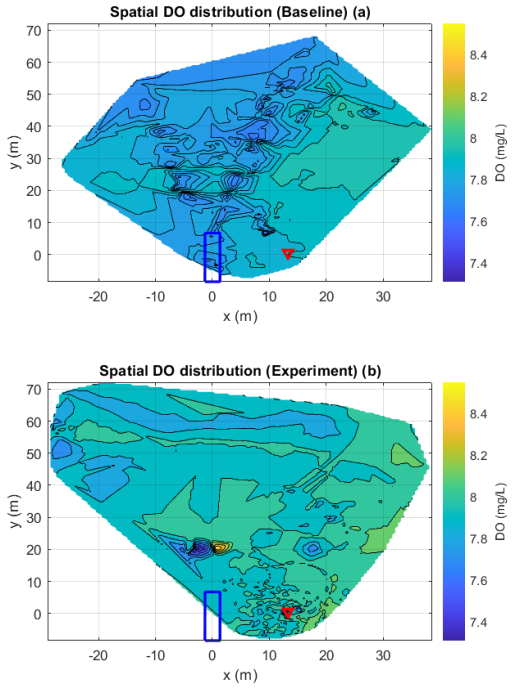

Fig. 18. Spatial distribution of the salinity values for the baseline (upper) and the experiment (lower) data

The spatial distribution of the DO values of the baseline and the experiment data are shown in Fig. 18. It can be observed from Fig. 18 that the spatial distribution of the DO changed during the experiments. Before the experiments, there were areas with low DO values between position $x = 0$ m $y = 20$ m and $x = 10$ m $y = 50$ m. However, the DO values did not change in other parts of the area, e.g. the area around position $x = 25$ m $y = 35$ m. Due to interpolation over the total experiment time, information about gradients may be generalized.

In order to determine the temporal change of the DO and to focus on the influence of the ASGD, the four time-equal segments, as depicted in Fig. 13, are considered in their spatial domain (Fig. 19). It can be observed from Fig. 19, that the DO value may be affected by the inflow of the ASGD, i.e. the DO near the ASGD position decreased over time during quarter two (Fig. 19 (b)). During the third and the fourth quarter, no decrease near the ASGD was observed. However, in both third and fourth quarters, other regions, which are in proximity to the ASGD, show a decrease in the values of DO, marked by red dashed rectangles (Fig. 19 (c) and (d)). The position of the spots are at $x_3 = 3.5$ m and $y_3 = 10.5$ m and $x_4 = 8.0$ m and $y_4 = -2.5$ m.

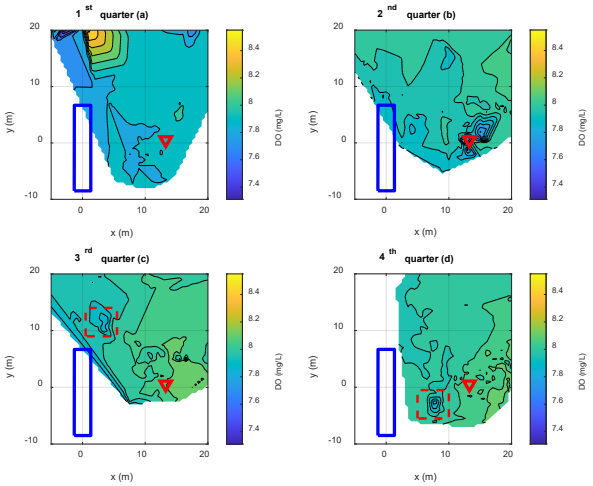

Fig. 19. Section of the spatial distribution of the DO focused on the area of the ASGD at different times during the experiment

V. Discussion

Six parameters were measured during the experiments: T, pH, ORP, EC, DO and FDOM. The experiments show, in accordance with [14], that temperature is not a suitable tracer for SGDs in shallow waters due to the influence of solar radiation.

Furthermore, although the EC-probe was calibrated, the recorded values seems to be too low. After post-calibration, the values are slightly higher than expected. A change in the internal resistance of the EC-probe between the *in-situ* measurements and the post-calibration might be the cause of this.

Against the assumption and the previous results of other researchers [6], the EC value seems to be unaffected by the inflow of the ASGD. A possible reason for this observation may be an insufficient inflow rate, not allowing stable EC gradients. Another possible explanation could be the response time of the EC sensor. Due to the movement of the ROV during data capture, the response time of the sensors plays a key role in order to detect gradients. To determine the response time of the EC sensor, a laboratory test using a tracer was carried out. The results of this test are shown in Fig. 20. It can be observed from Fig. 20, that it takes about four seconds for the sensor to respond. Taking into account the maximum speed of the ROV (v_{max} = 1 m/s), it might be possible that the sensor was not able to measure the lower EC value during the travel of the ROV.

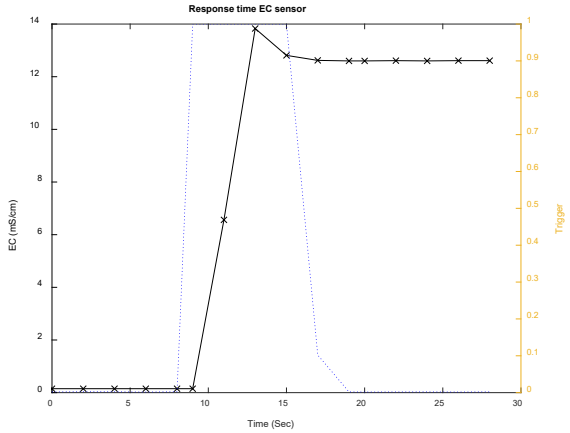

Fig. 20. Response of the EC sensor on a rapid change of the DO level in the environment

The position estimation using an acoustic based system was affected by several sources of error, such as multipath propagation, variable speed of sound or error-prone receiver positioning. This results in an error budget, significantly higher than the one of satellite positioning systems, such as GPS [9]. Furthermore, the environment may affect the positioning system used, as shown in Fig. 4 and Fig. 5. The pillar of the jetty for example seems to shadow some of the receivers whilst the ROV is moving through the area. In some cases, this might result in large positioning errors. These positioning uncertainties have direct negative impact on the calculation of the spatial distribution of the recorded data. Assuming a systematic positioning offset, it appears well possible that the recognized DO decreases in quarters three and four (Fig. 19) indicate the ASGD. The distances from the detected sinks to the true ASGD position are d_3 = 14 m for quarter three and d_4 = 6.1 m for quarter four.

Furthermore, there might be other sources of freshwater in the area under investigation besides the ASGD. In addition, neither the effects of tides nor solar radiation effects were addressed during the survey.

VI. Conclusion and Future Work

In this research, the spatial distribution of discharged freshwater from ASGDs was investigated. It was shown during the experiments, that the developed sensor system can be used to investigate the spatial distribution of discharged freshwater. However, the reported positons of the positioning system seems to be error-prone. In order to determine the accuracy of the used positioning system, conducting experimental tests and simulations on the accuracy of the system is recommended. In addition, other internal sensors of the vehicle, like an inertial measurement unit (IMU), can be fused with the acoustic system using Extended Kalman Filter or a Particle Filter in order to increase the reliability of the position estimation [9].

The EC readings are biased due to a change in the resistance of the electronic circuit. However, even if the other parameter readings seems to be unaffected, it cannot be guaranteed, that the readings of the ORP, pH and DO sensors are correct, since they are connected in the same way as the EC sensor. In the current configuration, the sensor boards are connected via plug-

in contacts, due to maintenance reasons. This might be the reason for the error. This probably led to a change of the electrical resistances of the contacts during a previous survey under sea conditions. However, for further surveys the system design should be modified, in order to ensure the sensor reliability.

Furthermore, machine-learning techniques might be able to extract relations between the different parameters, in order to increase the possibility of detecting SGDs.

In addition, the data gathered during these experiments will provide the basis to fine-tune search algorithms for AUVs using a simulation based on a Cellular Automaton [15]. Eventually, the designed search algorithms potentially could be used to search for SGDs in unknown areas.

REFERENCES

[1] C. Tholen, L. Nolle, T. El-Mihoub, O. Zielinski and J. Wellhausen, "Development of an intelligent and distributed low-cost platform for marine observations," *OCEANS 2019 - Marseille,* pp. 1-6, 2019.

[2] W. Moore, "The effect of submarine groundwater discharge on the ocean," *Annual Review of Marine Science, Vol. 2,* pp. 59-88, 2010.

[3] O. Zielinski, J. Busch, A. Cembella, K. Daly, J. Engelbrektsson, A. Hannides and H. Schmidt, "Detecting marine hazardous substances and organisms: sensors for pollutants, toxins and pathogens," *Ocean Science, Vol. 5,* pp. 329-349, 2009.

[4] T. Evans and A. Wilson, "Groundwater transport and the freshwater–saltwater interface below sandy beaches," *Journal of Hydrology, 538,* p. 563–573, 2016.

[5] J. L. Kelly, H. Dulai, C. R. Glenn and P. G. Lucey, "Integration of aerial infrared thermography and in situ radon-222 to investigate submarine groundwater discharge to Pearl Harbor, Hawaii, USA," *Limnology and Oceanography. 9999,* pp. 1-20, 2018.

[6] C. M. Richardson, H. Dulai, B. N. Popp, K. Ruttenberg and J. K. Fackrell, "Submarine groundwater discharge drives biogeochemistry in two Hawaiian reefs," *Limnol. Oceanogr., 62:,* p. 348–363, 2017.

[7] C. Tholen, T. El-Mihoub und L. Nolle, „On the robustness of self-adaptive Levy-flight," in *2018 OCEANS - MTS/IEEE Kobe Techno-Oceans (OTO)*, Kobe (Japan), 2018.

[8] H. Dulaiova, R. Peterson, W. C. Burnett and D. Lane-Smith, "A multi-detector continuous monitor for assessment of 222 Rn in the coastal ocean," *J Radioanal Nucl Chem 263 (2),* p. 361–363, 2005.

[9] L. Paull, S. Saeedi, M. Seto and H. Li, " "AUV Navigation and Localization: A Review,"," *IEEE Journal of Oceanic Engineering, vol. 39, no. 1,* pp. 131-149, 2014.

[10] NXP Semiconductors, I2C-bus specification and user manual Rev. 6, NXP Semiconductors, 2014.

[11] P. Kowalczuk, M. Zabłocka, S. Sagan and K. Kuliński, "Fluorescence measured in situ as a proxy of CDOM absorption and DOC concentration in the Baltic Sea," *OCEANOLOGIA, 52(3),* p. 431–471, 2010.

[12] WTW GmbH, „inoLab 740 Operating Manual," [Online]. Available: https://www.xylemanalytics.com/en/File%20Library/Resource%20Library/WTW/01%20Manuals/ba75530e03_inoLab_740_Box.pdf. [Zugriff am 09 06 2020].

[13] UNESCO, "Algorithms for computation of fundamental properties of seawater," *Unesco technical papers in marine sciences (44),* 1983.

[14] C. Stedmon, C. Osburn und T. Kragh, „Tracing water mass mixing in the Baltic–North Sea transition zone using the optical properties of coloured dissolved organic matter," *Estuarine, Coastal and Shelf Science, 87(1),* p. 156–162, 2010.

[15] C. Tholen, T. El-Mihoub, J. Dierks, L. Nolle, A. Burger and O. Zielinski, "Automated Tuning Of A Cellular Automata Using Parallel Asynchronous Particle Swarm Optimisation," *Proceedings of the 33rd International ECMS Conference on Modelling and Simulation,* pp. 30-36, 2019.